

Electrodynamics of binary neutron star mergers

Maxim Lyutikov

*Department of Physics, Purdue University, 525 Northwestern Avenue, West Lafayette, IN
47907-2036*

ABSTRACT

We consider electromagnetic interaction and precursor emission of merging neutron stars. Orbital motion of the magnetized neutron star may revive pair production within the common magnetosphere years before the merger, igniting pulsar-like magnetospheric dynamics. We identify two basic scenarios: (i) only one star is magnetized (1M-DNS scenario) and (ii) both stars are magnetized (2M-DNS scenario). Inductively created electric fields can have component along the total magnetic field (gaps) and/or the electric field may exceed the value of the local magnetic field. The key to the detection is orbital modulation of the emission. If only one star is magnetized (1M-DNS scenario) the emission is likely to be produced along the direction of the magnetic field at the location of the secondary; then, if the magnetic axis is misaligned with the orbital spin, this direction is modulated on the orbital period. For the 2M-DNS scenario, the structure of the common magnetosphere of the non-rotating neutron stars is complicated, with gaps, but no $E > B$ regions; there is strong orbital variations for the case of misaligned magnetic moments. For the same parameters of neutron stars the 2M-DNS scenario has intrinsically higher potential than the 1M-DNS one. The overall powers are not very high, $\leq 10^{45}$ erg s $^{-1}$; the best chance to detect electromagnetic precursors to the merging neutron stars is if the interaction of their magnetospheres leads to the production of pulsar-like coherent radio emission modulated at the orbital period, with luminosity of up to ~ 1 Jankys at the time the merger.

Subject headings: Physical Data and Processes: acceleration of particles, magnetic fields, plasmas; Stars: gamma-ray burst: general

1. Introduction: expected precursors to DNS mergers

The detection of gravitational waves associated with a GRB (Abbott et al. 2017) identifies merger of neutron stars as the central engine. It is highly desirable to detect any possible precursor to the main event. At the time of the merger the electromagnetic interaction of the neutron stars can be considered as interaction of magnetized dipole(s), §2. Hansen & Lyutikov (2001) (see also Lai 2012) argued that magnetospheric interaction during double neutron star (DNS) merger can lead to the production of electromagnetic radiation. The underlying mechanism advocated in those

works is a creation of inductive electric field due to the relative motion of one NS, assumed to be unmagnetized, in the magnetic field of the companion (Goldreich & Julian 1969; Lyutikov 2011b). Below we call it the 1M-DNS case, §3.

Typically simulations of the DNS merger with magnetic field is done within the MHD approximation (*e.g.* Palenzuela et al. 2013b,a; Ponce et al. 2014, 2015; Baiotti & Rezzolla 2017). These simulations are well suited to understanding the overall structure of the interacting magnetospheres. But they do not capture the dissipative/acceleration process. In MHD (even with resistivity) the formation of gaps is prohibited. Thus, such simulations will miss the effects we discuss below - formation of gaps and dissipative regions with $E > B$. We develop a complimentary electromagnetic model of interacting magnetospheres, based on the pulsar magnetosphere model of Goldreich & Julian (1969).

We expect that gaps forming in the magnetosphere of interacting neutron stars are not sustainable for a long time: if they create pairs the resulting charge separation screens the parallel electric field, often in a non-stationary way (Levinson et al. 2005; Timokhin 2010). As a result, the magnetospheric structure would generally evolve towards ideal MHD limit (without parallel component of the electric field), with a network of current sheets. Simulations of Palenzuela et al. (2013b) do show strong magnetospheric interaction and formation of current sheets. Particles accelerated in reconnection events at these current sheets (*e.g.* Lyutikov et al. 2018) can also produce unstable distribution and coherent radio emission.

In this paper we first consider the structure of the common magnetosphere within the 1M-DNS model and then point out that the interaction of the magnetospheres of the two *magnetized* neutron stars - 2M-DNS scenario- will produce more powerful emission, §4. Most importantly, in both cases we expect orbital-dependent emission pattern, that is a key to a possible future detection.

2. Orbital resurrection of the rotationally dead

A neutron star after a time t_{NS} since birth will have a spin period (Goldreich & Julian 1969)

$$\Omega_{NS} \approx \frac{c^{3/2} \sqrt{I_{NS}}}{\sqrt{2} \sqrt{t_{NS}} B_{NS} R_{NS}^3} = 0.7 \text{ rad s}^{-1} t_{NS,9}^{-1/2}, \quad (1)$$

where the surface magnetic field $B_{NS} = 10^{12}$ G is assumed, $t_{NS,9}$ is time in gigayears; $I_{NS} \approx 10^{45}$ g cm² is the moment of inertia, $R_{NS} = 10$ km is neutron star radius. Thus in a giga-year a star spins down to ~ 10 seconds.

The electric potential Φ_{spin} due to pulsar spin is (Goldreich & Julian 1969)

$$\Phi_{spin} \approx \frac{\Omega^2 B_{NS} R_{NS}^3}{c^2} = 100 t_{NS,9}^{-1} \text{ GeV} \quad (2)$$

Typically, vacuum breakdown occurs at $\Phi \geq 100$ GeV (Fawley et al. 1977; de Jager et al. 1996; Hirschman & Arons 2001; Timokhin 2010). Thus the merging neutron stars are likely to be dead

pulsars, with no pair production within their magnetospheres. (There is an apparent exception to this, Tan et al. 2018)

At the orbital separation r the time to merger ($-t$) is (Misner et al. 1973)

$$-t \approx \frac{c^5 r^4}{(GM_{NS})^3} \quad (3)$$

The light cylinder $R_{LC} = c/\Omega_{NS}$ becomes smaller than the orbital size at time ($-t_{LC}$)

$$(-t_{LC}) = \frac{4c^3 B_{NS}^4 R_{NS}^{12} t_{NS}^2}{G^3 I_{NS}^2 M_{NS}^3} = 5 \times 10^8 \text{ yrs} \quad (4)$$

Thus for a few hundred million years the neutron stars are within each other's magnetosphere, so that their interaction can be considered as an interaction of either a vacuum dipole with a highly conducting sphere (if only one star is magnetized) or two vacuum dipoles. At this point stars are separated by $5 \times 10^{10} t_{NS,9}^{1/2}$ cm. (Also, the light cylinder for the orbital motion when stars are separated by r is located at

$$R_{LC} \sim \frac{cr^{3/2}}{\sqrt{GM}} = \frac{G^{5/8} (-t)^{3/8} M_{NS}^{5/8}}{c^{7/8}} = 2 \times 10^7 (-t)^{3/8} \quad (5)$$

This is much larger than the size of the orbit until the final merger.)

As the stars spiral in, the magnetospheres can be revived due to relative motion of the magnet(s). On basic grounds (Blandford 2002; Lyutikov 2006), if a system has typical magnetic field B , internal velocity $v = \beta c$ and typical size R , the electric potential and electromagnetic luminosity can be estimated as

$$\begin{aligned} \Phi &\sim \beta B R \\ L &\sim \Phi^2 c \end{aligned} \quad (6)$$

In this paper we discuss two cases that both employ relations (6), but in somewhat different regime: Single-magnetized DNS (1M-DNS) and Double-magnetized DNS (2M-DNS) mergers. The case of 1M-DNS is akin to a conductor moving in magnetic field - there is then an induced electric field, mostly close to the conductor's/neutron star's surface, that induces *a la* Goldreich-Julian surface charges, that create parallel electric field, that leads to particle acceleration. In addition - this is different from the pulsar magnetosphere case - regions with $E > B$ can be created. Like in case of pulsars, regions with $\mathbf{E} \cdot \mathbf{B} \neq 0$ and $E > B$ will lead to particle acceleration, pair production, and shortening of the acceleration electric field, most likely in a non-stationary way (Levinson et al. 2005).

The case of 2M-DNS involves interacting relativistic magnetospheres - here the stars play a role of the point dipoles that produce electromagnetic fields in their surrounding. Those electromagnetic

fields can form gaps and/or reconnecting current sheets, leading to energization, acceleration of particles, and production of non-thermal and possibly coherent radio emission.

The power and the available potential in both cases of 1M-DNS and 2M-DNS scenarios can be estimated using (6) with typical magnetic field due to a dipole at the distance of orbital separation $B \sim B_{NS}(r/R_{NS})^{-3}$ and typical radius $R = R_{NS}$ in case 1M-DNS (Eq. (7)) and $R = r$ in the case 2M-DNS (Eq. (23)).

Typically, there is enough potential (see Eqns. (7) and (23)) to start pair production at times before merger ($-t$) $\sim 10^{12}$ seconds, $\sim 5 \times 10^4$ years. At that moment the stars are separated by $\sim 5 \times 10^9$ cm. Starting this moment we may expect some electromagnetic signal from the system.

As we discuss below, most of the common magnetosphere remains open, so that we do not expect large stationary regions filled with plasma, like in the case of pulsar’s closed field lines (Goldreich & Julian 1969). Also, pair production is likely to be intermittent. Thus, a vacuum approximation is expected to be a reasonable approximation.

Let us consider the electromagnetic structure of two interacting vacuum DNS magnetospheres. Following of the classic work of Goldreich & Julian (1969), we will find that orbiting neutron stars create electric potentials along the combined electric fields. This serves as a first-order approximation to the expected nearly ideal plasma, that at the same time has special accelerations regions with $\mathbf{E} \cdot \mathbf{B} \neq 0$.

Let us next discuss cases 1M-DNS and 2M-DNS in detail.

3. Interacting DNS magnetospheres: 1M-DNS case

If only one star is magnetized, we are dealing with a metal sphere (second neutron star) moving through the magnetic field of the primary. This was the case originally considered by Hansen & Lyutikov (2001). Below in this section we provide a more detailed description of the resulting interaction.

3.1. 1M-DNS: estimates of power

If a neutron star is moving in the field of a primaries’ dipolar magnetic field at orbital separation r , the induced potential and the corresponding powers are (Hansen & Lyutikov 2001; Lyutikov 2011a)

$$\begin{aligned} \Phi_1 &\sim BR_{NS} = \frac{B_{NS}R_{NS}^4\sqrt{GM_{NS}}}{cr^{7/2}} = 10^{18}(-t)^{-7/8} \text{ eV} \\ L_1 &\sim \frac{GB_{NS}^2M_{NS}R_{NS}^8}{cr^7} = 3 \times 10^{41}(-t)^{-7/4} \text{ erg s}^{-1} \end{aligned} \tag{7}$$

where in the last relations the time to merger t is measured in seconds. (Index 1 indicates here that the interaction is between single magnetized neutron star and unmagnetized one.)

3.2. 1M-DNS - internal structure of the magnetosphere

Consider a highly conducting unmagnetized neutron star moving through the magnetic field of the companion. The expected parallel electric field that would develop in the system will be largest near the surface of the companion (unmagnetized) neutron star. Hence, for simplicity we approximate the dipolar magnetic field of the primary at the location of the secondary as a straight vertical field. This is a good approximation if the sizes of the stars are much smaller than the orbit.

The neutron star is highly conducting, and can be approximated as a conducting metal sphere, so that the magnetic field does not penetrate, Fig. (1). The induced field is

$$\begin{aligned} B_r &= -\frac{R^3}{r^3} \cos \theta B_0 \\ B_\theta &= \frac{R^3}{r^3} \sin \theta B_0 \end{aligned} \quad (8)$$

while the total magnetic field is

$$\begin{aligned} B_r &= -\left(1 - \frac{R^3}{r^3}\right) \cos \theta B_0 \\ B_\theta &= \frac{1}{2} \left(2 + \frac{R^3}{r^3}\right) \sin \theta B_0 \end{aligned} \quad (9)$$

The conducting sphere is sliding through the magnetic field with the relative velocity

$$\mathbf{v} = 2\Omega \times \mathbf{r} \quad (10)$$

(here r is a semi-major axis). As a result magnetic field in the observer frame is time-dependent: there is non-zero $\partial_t \mathbf{B}$, which would produce electric field. The resulting electric field will generally have a component parallel to the magnetic field.

Below, in §3.3 we first consider a case of the secondary neutron star moving orthogonally (in the equatorial plane of the primary) through the magnetic field of the primary. Later, §3.4, we generalize to oblique propagation.

3.3. 1M-DNS - motion of the secondary in the magnetic equatorial plane of the primary

let us first consider the case when the secondary unmagnetized star is moving perpendicular to the magnetic field lines. In Eq. (9) make a transformation to the observer frame by writing

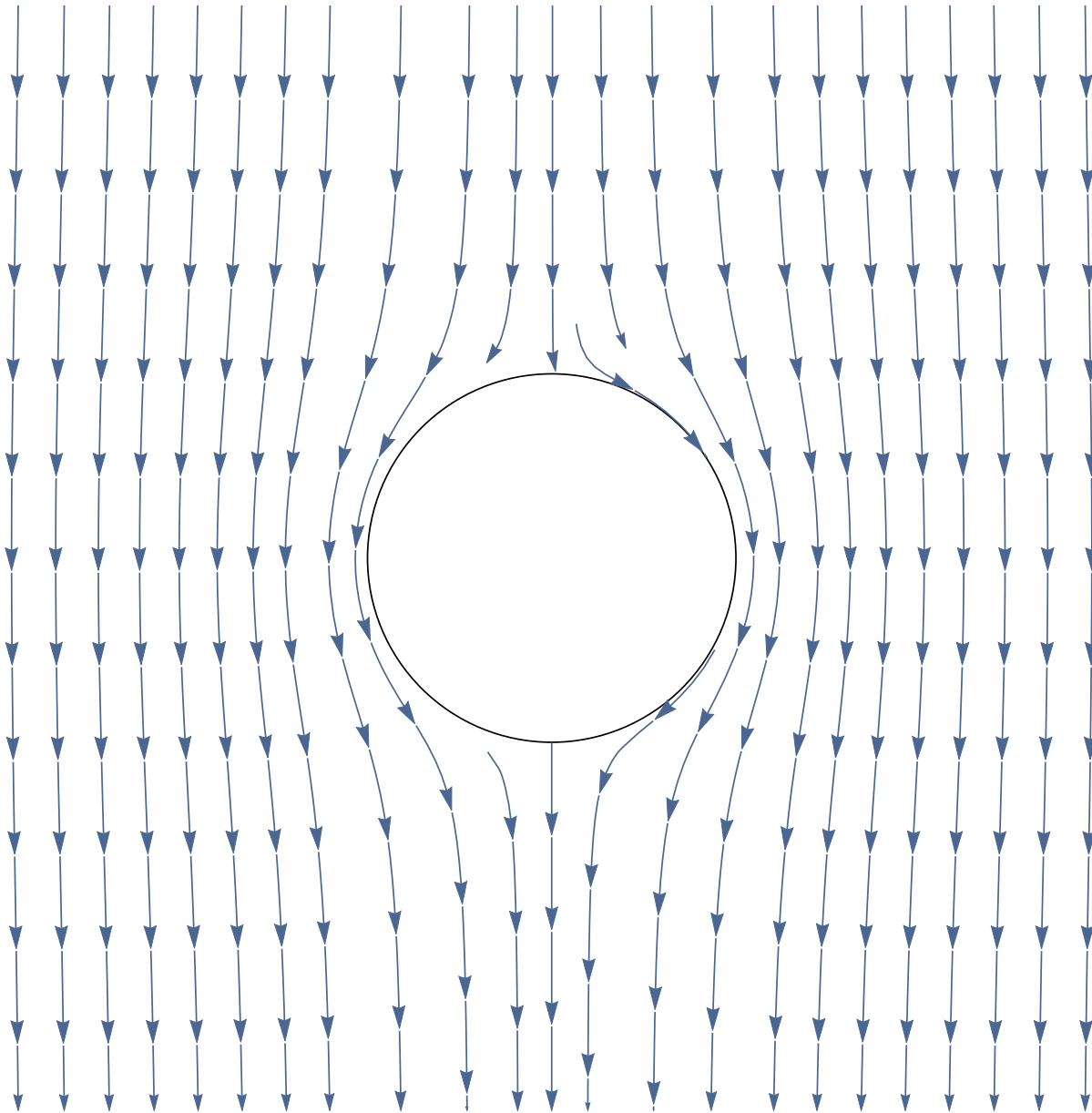


Fig. 1.— Expulsion of the magnetic field by a conducting sphere.

$y \rightarrow y + \beta_0 t$. Time derivative of (9) (evaluated at arbitrary $t = 0$) is

$$\partial_t \mathbf{B} = \left\{ -\frac{9}{4} \sin 2\Theta \sin \phi, \frac{3}{2} \cos 2\Theta \sin(\phi), \frac{3}{2} \cos \Theta \cos \phi \right\} \frac{\beta_0 B_0 R^3}{r^4} \quad (11)$$

(in $\{r, \theta, \phi\}$ coordinates. This equals minus the curl of the induced electric field. We find a vacuum electric field with $\text{div } \mathbf{E} = 0$

$$\mathbf{E}_{ind} = - \left\{ \frac{1}{2} \sin \Theta \cos \phi, -\cos \Theta \cos \phi, \frac{1}{4}(3 \cos(2\theta) + 1) \sin \phi \right\} \frac{\beta_0 B_0 R^3}{r^3} \quad (12)$$

(alternatively, we could do a Lorentz boost of the induced magnetic field (8), giving the same result).

The induced field \mathbf{E}_{ind} (12) has a component normal to the surface of the NS, that will produce surface charge density σ

$$E_{ind,r}|_{r=R} = -\frac{1}{2} \sin \Theta \cos \phi B_0 v = 4\pi\sigma \quad (13)$$

The surface charge will produce an electric field

$$\mathbf{E}_s = \left\{ \frac{1}{2} \sin \Theta \cos \phi, -\frac{1}{4} \cos \Theta \cos \phi, \frac{1}{4} \sin \phi \right\} \frac{\beta_0 B_0 R^3}{r^3} \quad (14)$$

The total field outside is then

$$\mathbf{E}_{tot} = \mathbf{E}_{ind} - \mathbf{E}_s = \left\{ -\sin \Theta \cos \phi, \frac{5}{4} \cos \Theta \cos \phi, \frac{1}{4}(2 + 3 \cos 2\Theta) \sin \phi \right\} \frac{\beta_0 B_0 R^3}{r^3} \quad (15)$$

The total magnetic and the electric fields (Eqns. (9) and (15)) have two important properties. They have non-zero first electromagnetic invariant $\mathbf{E} \cdot \mathbf{B}$ and the second invariant $B^2 - E^2$ can change sign.

The parallel component of the electric field equals

$$E_{\parallel} = -\frac{3}{2\sqrt{2}} \frac{\sin \Theta \cos \Theta \left(6 - \frac{R^3}{r^3}\right) \cos(\phi)}{\sqrt{8 \left(1 - \frac{R^3}{r^3}\right)^2 + 6 \left(4 - \frac{R^3}{r^3}\right) \frac{R^3}{r^3} \sin^2 \Theta}} B_0 \beta \left(\frac{R}{r}\right)^3. \quad (16)$$

Fig. 2 shows that there are regions of non-zero parallel electric field, peaking in value close to the neutron star surface. If plasma is generated in these regions, the outflows will be directed mostly along the external magnetic field, passing close to the poles.

The parallel electric field is maximal in the $y = 0$ plane ($\phi = 0, \pi$). At each $r \neq R$ the maximal values of E_{\parallel} is reached at $\cos^2 \theta = (2r^3 + R^3)/(4r^3 - R^3)$. At $r \rightarrow R$ this corresponds to $\theta = 0, \pi$, where the total magnetic field is zero.

The invariant $B^2 - E^2$ equals

$$B^2 - E^2 = \frac{1}{16} \left(\left(16 \left(1 - \frac{r^3}{R^3} \right)^2 - 25\beta^2 \cos^2(\phi) \right) \cos^2(\Theta) + 4 \left(\left(\frac{2r^3}{R^3} + 1 \right)^2 - 4\beta^2 \cos^2(\phi) \right) \sin^2(\Theta) \right. \\ \left. - \beta^2 (3 \cos(2\Theta) + 2)^2 \sin^2(\phi) \right) \frac{R^6}{r^6} B_0^2 \quad (17)$$

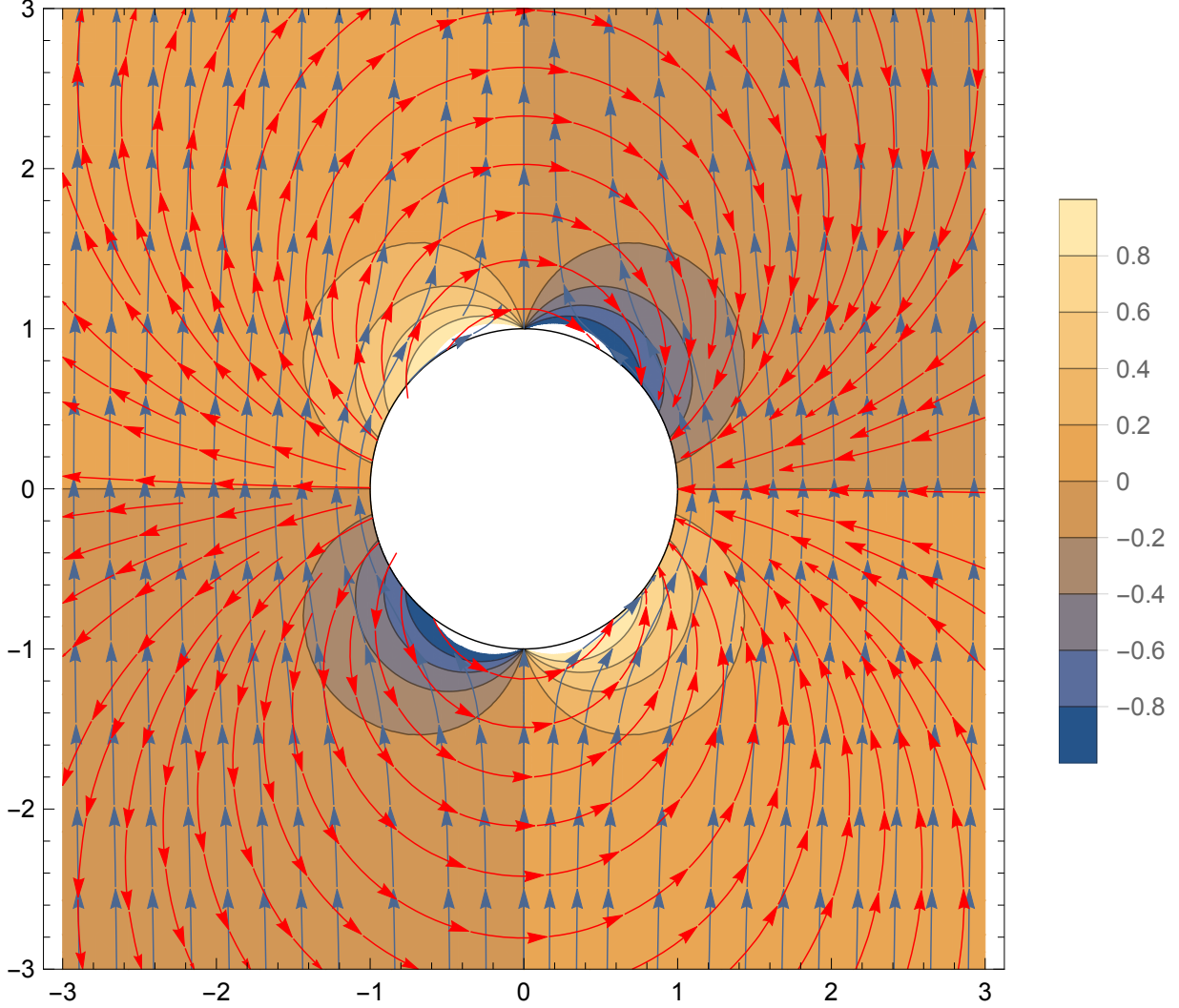


Fig. 2.— Magnetic field lines (blue arrows), total electric field (red arrows) and the value of \mathbf{E}_{\parallel} (in color) in the plane $y = 0$ for a metal sphere of radius R moving in constant magnetic field. Electric field is measured in units $B_{NS}\beta R^3$ and coordinates in r/R .

It becomes negative within a dome-like structure near the poles. On the surface of the neutron star it is < 0 within a region

$$\cos^2 \phi = \frac{36 \sin^2(\Theta) - \beta^2(3 \cos(2\Theta) + 2)^2}{3\beta^2 \sin^2(\Theta)(6 \cos(2\Theta) + 11)} \quad (18)$$

(for each value of ϕ Eq. (18) gives the value of θ so that for smaller θ (closer to the pole) we have $B < E$, see Fig. 3). Note that even in the $\phi = \pi/2$ plane, where the electric field is zero, the magnetic field is also zero, so that the the second invariant remains negative close to the poles. At the poles, $\theta = 0, \pi$, on the surface $B^2 - E^2 = -(25/16)B_0^2\beta^2$; the region extends to

$$r/R = (1 + (5/4)\beta)^{1/3}.$$

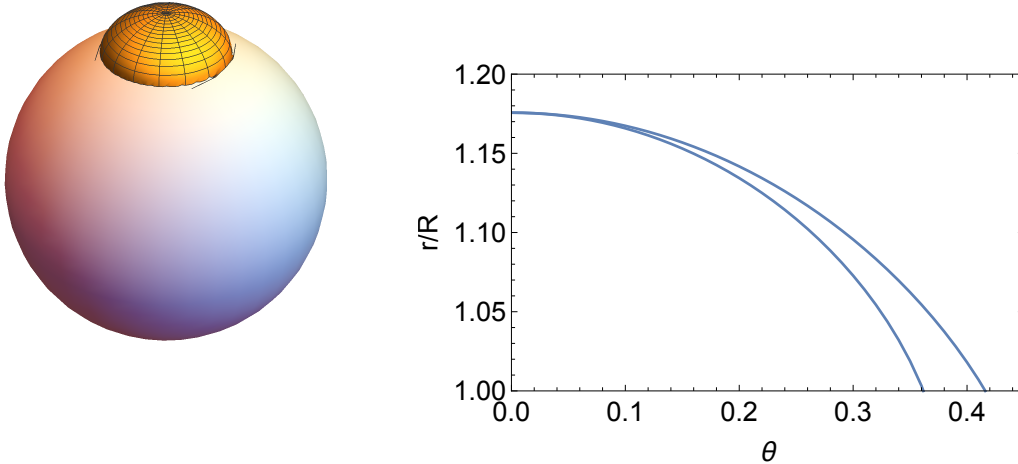


Fig. 3.— (Left panel) 3D rendering of the regions with $B < E$. The region is slightly non-circular: the right panel shows cross-section in the $\phi = 0$ plane (top curve) and $\phi = \pi/2$ plane for $\beta = 0.5$.

It is expected that both the conditions $\mathbf{E} \cdot \mathbf{B} \neq 0$ and $B^2 < E^2$ will lead to particle acceleration. This might create conditions favorable for the generation of coherent radio emission. Without a particular global model of particle acceleration we cannot predict in detail the expected radio signal. Both the region $B < E$ and the region with the largest E_{\parallel} are concentrated near the pole, so that in the case of motion in the equatorial plane, no variation is expected.

The above results can be compared with the case of a black hole moving through straight magnetic field (Palenzuela et al. 2010; Lyutikov 2011b). In that case two dual jets are generated. As Fig. 2 demonstrates, in the case of moving metal sphere the configuration looks similar: there are four regions with high parallel electric field.

3.4. 1M-DNS - oblique motion of the secondary

Above, in §3.3 we considered the motion of the secondary unmagnetized neutron star in constant magnetic field, a case applicable to when the magnetic moment of the primary is along the orbital spin. Next we generalize it to the oblique orbits of the secondary (inclined magnetic moment of the primary).

In the case of the oblique motion (not orthogonal to the spin) we can separate the motion along and across the magnetic field. For the part of motion along the external magnetic field, we

find

$$E_\phi = -\frac{3\beta B_0 R^3 \sin(2\theta)}{4r^3} \quad (19)$$

Thus, this does not create a component of electric field along the magnetic field. Also, the second electromagnetic invariant

$$B^2 - E^2 = \left(\frac{12 \cos(2\theta) + 20}{32r^6} + \frac{9v^2(\cos(4\theta) - 1)}{32r^6} \right) B_0^2 R^6 \quad (20)$$

is always positive.

Thus what counts for the producing emission regions ($\mathbf{E} \cdot \mathbf{B} \neq 0$ or $B < E$) is the component of the velocity perpendicular to the magnetic field. Since the primary is assumed non-rotating, only the component of the velocity perpendicular to the magnetic moment of the primary is of importance. As we argued above, the emission is likely to be produced along the magnetic field at the location of the secondary.

Consider a dipole of the primary inclined by the angle Θ with respect to orbit normal, located at the origin, $\{0, 0, 0\}$. The secondary at time t is located at $x_0\{\cos \Omega t, \sin \Omega t, 0\}$ (in Cartesian coordinates $\{x, y, z\}$, where Ω is the orbital frequency). At the location of the secondary, the direction of the primary's magnetic field is

$$\mathbf{B}_{1-2} = \{-\sin \Theta(3 \cos 2\Omega t + 1), -3 \sin \Theta \sin 2\Omega t, 2 \cos \Theta\} \frac{1}{\sqrt{-6 \cos 2\Theta \cos^2 \Omega t + 3 \cos 2\Omega t + 7}} \quad (21)$$

in $\{x, y, z\}$ coordinates. The direction of emission varies on the orbital time scale. Thus, if emission is generated near the secondary along the local direction of the magnetic field of the primary we expect modulation of the direction on orbital time scale.

4. Interacting DNS magnetospheres: 2M-DNS case

4.1. 2M-DNS - general notes

Next we study the interaction of two dipoles that are moving with respect to each other with the (Keplerian) velocity $v = \beta c$. We can identify 4 basic geometries: (i-a) magnetic moments aligned with the orbital spin axis; (i-b) magnetic moments anti-aligned with the orbital spin axis; (ii-a) one magnetic moment is aligned with the orbital spin axis and another is along the line connecting the two neutron stars; (ii-b) one magnetic moment is aligned with the orbital spin axis and another is orthogonal both to the orbital axis and the line connecting the two neutron stars. Surely, there more complicated structures when both magnetic moments are misaligned, but these four, we think, cover the basics.

Qualitatively, cases i-a and i-b produce nearly time independent signals and are less of interest (in this case the procedure described below implies that the maximal emission is produced along

the z -axis, though at different orbital phases the line of sight does pass through different regions). Cases ii-a and ii-b are dynamically related - a system of neutron stars where one neutron star is aligned with the orbital spin and the spin of the order is in the orbital plane will periodically evolve from ii-a to ii-b. As we demonstrate below, this will lead to considerably different magnetospheric structures and possibly time-dependent radiative signatures.

Consider two neutron stars of same masses and producing in the surrounding space magnetic fields \mathbf{B}_1 and \mathbf{B}_2 . Assume that the neutron stars are non-rotating - typical merger times are much longer than the typical spin-down times and orbital synchronization is not important (Bildsten & Cutler 1992). In the center of mass the star 1 is moving with velocity $\mathbf{v}_1 = \Omega \times \mathbf{r}_1$ and star 2 is moving with velocity $\mathbf{v}_2 = \Omega \times \mathbf{r}_2 = -\mathbf{v}_1$. Neglecting relativistic effects, they create the total magnetic field $\mathbf{B} = \mathbf{B}_1 + \mathbf{B}_2$ and the electric field $\mathbf{E} = -\mathbf{v}_1 \times \mathbf{B}_1 - \mathbf{v}_2 \times \mathbf{B}_2 = -\mathbf{v}_1 \times (\mathbf{B}_1 - \mathbf{B}_2)$. This total electric field has a component parallel to the total magnetic field:

$$\mathbf{E} \cdot \mathbf{B} = -(\mathbf{v}_1 \times (\mathbf{B}_1 - \mathbf{B}_2)) \cdot (\mathbf{B}_1 + \mathbf{B}_2) = -(\mathbf{v}_1 \times \mathbf{B}_1) \cdot \mathbf{B}_2 + (\mathbf{v}_1 \times \mathbf{B}_2) \cdot \mathbf{B}_1 = -2(\mathbf{v}_1 \times \mathbf{B}_1) \cdot \mathbf{B}_2, \quad (22)$$

which is generally non-zero. Thus, regions of non-zero parallel electric field will be created within the interacting magnetospheres.

4.2. 2M-DNS - estimates of power

In this paper we point out that *magnetospheric interaction* of two magnetized neutron stars can generate larger luminosity than the case of one star moving in the field of the other considered by Hansen & Lyutikov (2001), see also §3. Qualitatively, the relative motion of two neutron stars creates large scale electric field that generally has a component parallel to the total magnetic field. These large scale electric fields are on the orbital scale, so that

$$\begin{aligned} \Phi_2 &\sim \beta Br = \frac{B_{NS} \sqrt{GM_{NS}} R_{NS}^3}{cr^{5/2}} = \frac{c^{17/8} B_{NS} R_{NS}^3}{(-t)^{5/8} (GM_{NS})^{11/8}} = 4 \times 10^{18} (-t)^{-5/8} \text{ stat - V} \\ L_2 &\sim \frac{B_{NS}^2 GM_{NS} R_{NS}^6}{cr^5} = \frac{c^{21/4} B_{NS}^2 R_{NS}^6}{(-t)^{5/4} (GM_{NS})^{11/4}} = 6 \times 10^{42} (-t)^{-5/4} \text{ erg s}^{-1} \end{aligned} \quad (23)$$

(Index 2 indicates here that the interaction is between two magnetized neutron star.) The ratio of luminosities of the models 1M-DNS and 2M-DNS is

$$\frac{L_2}{L_1} = \left(\frac{GM}{c^2 R_{NS}} \right)^{3/2} \sqrt{\frac{(-t)c}{R_{NS}}} \approx 16\sqrt{-t} \quad (24)$$

Thus L_2 dominates L_1 prior to merger.

The power (23) is fairly small until the last few minutes. Even at the time of a merger, with $t \sim 10^{-2}$ seconds the corresponding power is only $L \sim 10^{45} \text{ erg s}^{-1}$ - amplification of magnetic field is needed to produce a typical GRBs with $L \sim 10^{50} \text{ erg s}^{-1}$.

If at the precursor stage the majority of the power comes out at soft photons with $\epsilon_{ph} \sim 1$ keV, the expected high energy photon flux at the Earth is

$$F = \frac{L_2}{4\pi d^2 \epsilon_{ph}} \sim 3 \times 10^{-3} (-t)^{-5/4} d_{100 \text{ Mpc}}^{-2} \text{ phot.s}^{-1} \text{ cm}^{-2} \quad (25)$$

It is smaller by few orders of magnitude than the detection limits of high energy satellites like Swift (Gehrels 2004).

The best case, we believe, is if a fraction of the power (23) is put into radio. If a fraction of η_R of the power is put into radio, the expected signal then is

$$F_R \sim \eta_R \frac{L_2}{4\pi d^2 \nu} \approx 0.1 \text{ Jy } \eta_{R,-5} (-t)^{-5/4} \quad (26)$$

This is a fairly strong signal that could be detected by modern radio telescopes. Of course, it's a transient source - but the power (26) is fairly large for a long time before the merger.

4.3. Case i: magnetic moments parallel to the orbital spin

Let us assume that the stars are located at coordinate $x = \pm x_0$ and are orbiting each other in the $x - y$ plane (so the orbital spin is along z-axis). (We neglect the sizes of the stars - the corresponding electromagnetic effects that take into account the size of the neutron stars were considered in §3). Below we will mostly plot 2D images in the $\{x - z\}$, $y = 0$ plane (defined by the spin axis and the line connecting the stars, in the plane of the stars) and the $\{y - z\}$, $x = 0$ plane (orthogonal to the line connecting the stars, passing through the center of mass). Results for the parallel case i are plotted in Fig. 4.

In the case of orbiting neutron stars with magnetic moments aligned with the orbital spin, there is some time dependence in the structure of the magnetosphere, but our prescription for estimating the preferred direction of the emission (see below) consistently predict emission along the spin axis, and hence no time variation. Nearly constant weak high energy or radio emission will be hard to detect observationally.

4.4. Case ii: one magnetic moment parallel to the orbital spin and another in the plane of the orbit

For this configuration the magnetic and electric fields are plotted in Fig. 5.

4.5. Case ii: time dependence

In contrast to the cases-i, the cases-ii are highly time dependent, as the system will evolve from ii-a, to ii-b, to “minus” ii-a, “minus” ii-b (by “minus” we mean the relative orientation of the

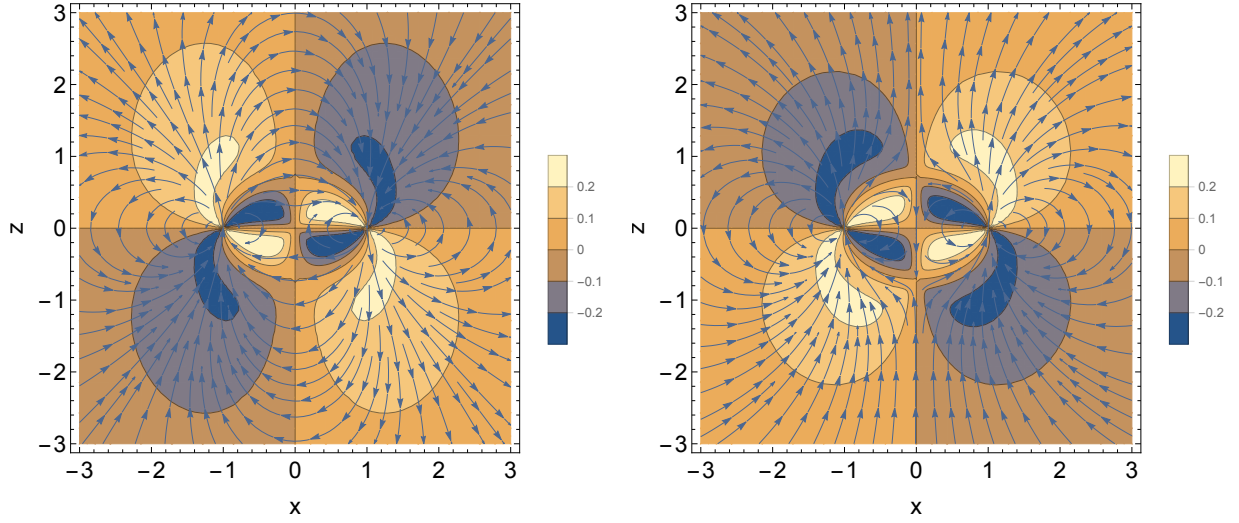


Fig. 4.— Case i: magnetic field lines (arrows) and the value of \mathbf{E}_{\parallel} (in color) for aligned (left) and misaligned (right) cases in the plane $y = 0$. Electric field is measured in units $B_{NS}\sqrt{GM_{NS}R_{NS}^3}/(cr^{7/2})$ where r is the semi-major axis of the orbit.

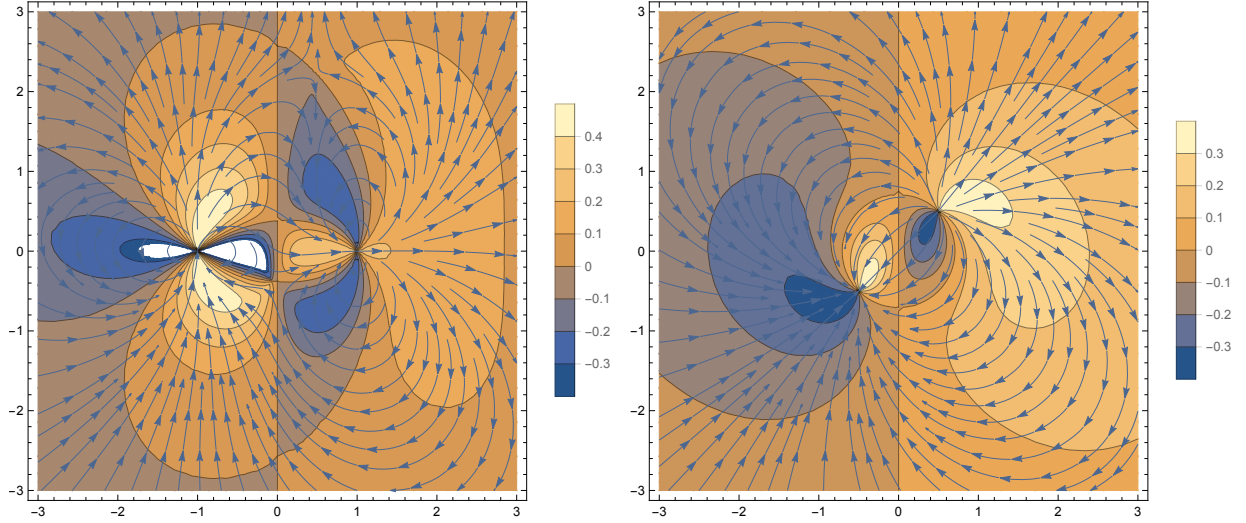


Fig. 5.— Case ii: magnetic field lines (arrows) and value of \mathbf{E}_{\parallel} (in color) for case ii-a in the plane $y = 0$ (containing the orbital spin and the two neutron stars). (left) and case ii-b (right) in the plane $x = 0$.

magnetic moment with respect to the line of sight). Thus, if the spins of the neutron stars are misaligned with the orbital spin, the structure of the magnetosphere will change quasi-periodically on the orbital time scale. This may result in periodically changing emission.

At the present state, we cannot predict radio emission properties given the macroscopic electro-

magnetic structure of the magnetosphere. Hence, we must resolve to probable emission indicators to predict the light curves. Let us choose the value of the parallel electric field as a proxy for the directional properties of radio emission. For any configuration we know $\mathbf{E} \cdot \mathbf{B}$, Eq (22) and Fig. 6. Let us assume that emission is produced along the magnetic field line at the point of maximal $\mathbf{E} \cdot \mathbf{B}$ within the magnetosphere. As a function of the polar angle θ and the azimuthal angle ϕ the resulting emission will have a complicated patten, Fig 7.

In both plots in Fig. 7 several curves arise because the code is looking for a global maximum but occasionally gets “trapped” in the local ones. This also indicates that emission may/could change sporadically, appearing at different field lines.

Finally, we note that in the 2M-DNS configuration $B^2 - E^2 \geq 0$ (it may become zero at some discreet number of point).

4.6. 2M-DNS - reconnection flares at corotation

If the stars are rotating, there is another possibility for the production of radiation due to linking of the two magnetospheres at the time when the orbital period matches the pulsar’s rotational period - at corotation. (Magnetospheric interaction in close RS CVn binaries, *e.g.* Uchida & Sakurai 1983, happens in this regime of near-corotation, whereby two stars can establish magnetic connections.)

Equating neutron star spin (1) with the orbital frequency at time $(-t)$ before the merger

$$\Omega \approx \frac{c^{15/8}}{G^{5/8}(-t)^{3/8}M_{NS}^{5/8}} \quad (27)$$

the corotating occurs at time

$$(-t_c) \approx \frac{ctNS^{4/3}B_{NS}^{8/3}R_{NS}^8}{I_{NS}^{4/3}(GM_{NS})^{5/3}} \approx 5 \times 10^8 \text{ sec} \quad (28)$$

At the time t_c the stars are separated by

$$r_c = \frac{t_{NS}^{1/3}B_{NS}^{2/3}(GM_{NS})^{1/3}R_{NS}^2}{cI_{NS}^{1/3}} \approx 5 \times 10^8 t_{NS,9}^{1/3} \text{ cm} \quad (29)$$

If two stars are in approximate corotation, there is time for magnetospheric field lines to reconnect, creating a link between the two stars. We stress that the stars become magnetically connected not due to the diffusive processes in the crust, but due to reconnection in the common magnetosphere, see Fig. 8.

After two stars established magnetic connection, the common field lines will be stretched due to (small) mismatch in the corotation condition. This mechanism puts some of the energy of the

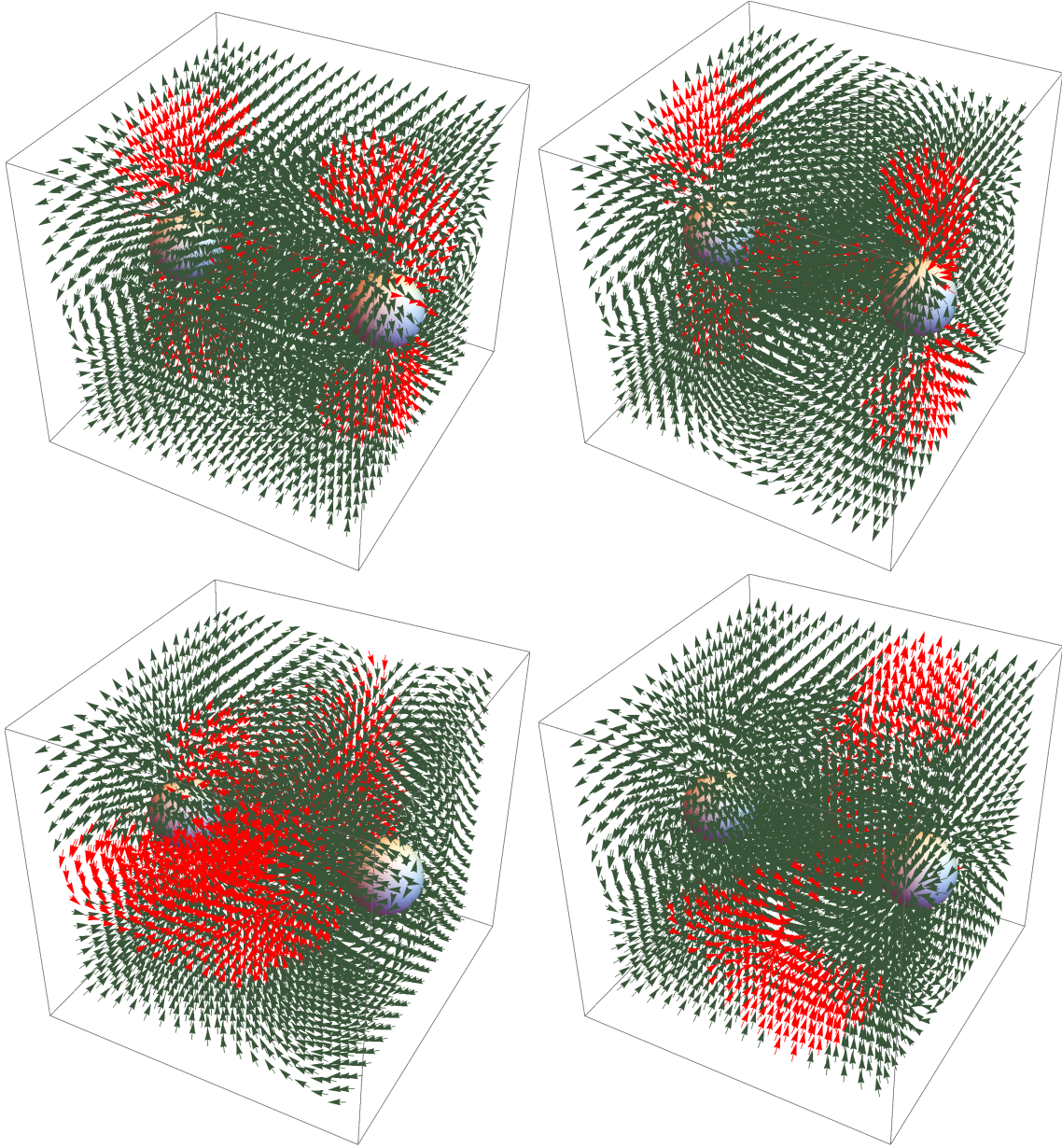


Fig. 6.— 3D rendering of the common magnetosphere of the interacting neutron stars for four basic orientation of dipoles. Shown are aligned (top left), anti-aligned (top right), and two orthogonal cases: one of the dipoles in the plane of the orbital spin and line connecting the stars ($x - z$ plane; low left), and perpendicular one (low right). Highlighted in red are regions with high parallel electric field. (Since in the orthogonal cases the parallel electric field is larger in absolute value than in the parallel/anti-parallel cases different criteria were used to highlight large E_{\parallel} regions in different configurations.

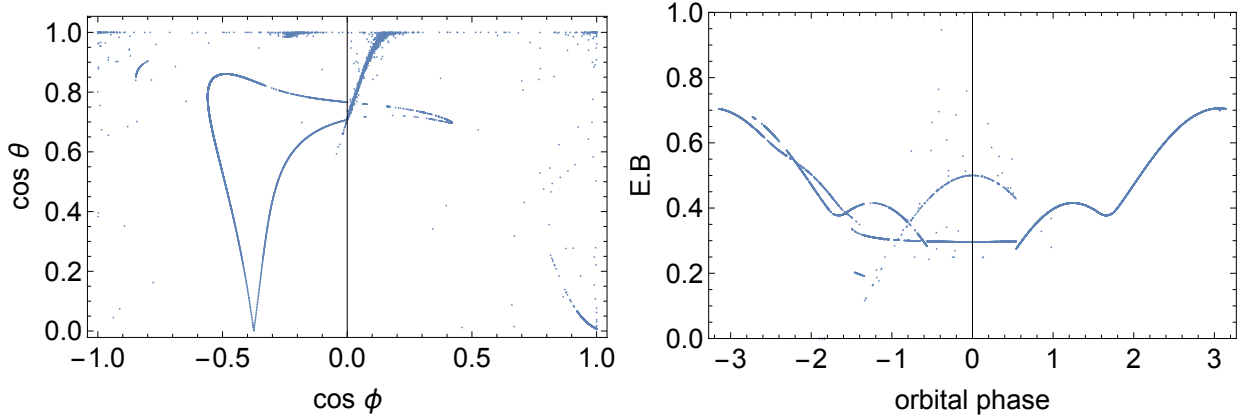


Fig. 7.— Interaction of the orthogonal dipoles. One dipole is aligned with the rotational axis, another is in the orbital plane. Left panel: Expected emission pattern (defined as a direction of the magnetic field at the point where $E_{||}$ is maximal) as a function of polar angle θ and azimuthal angle ϕ . Right panel: maximal value of $E_{||}$ as a function of orbital phase of the two neutron stars.

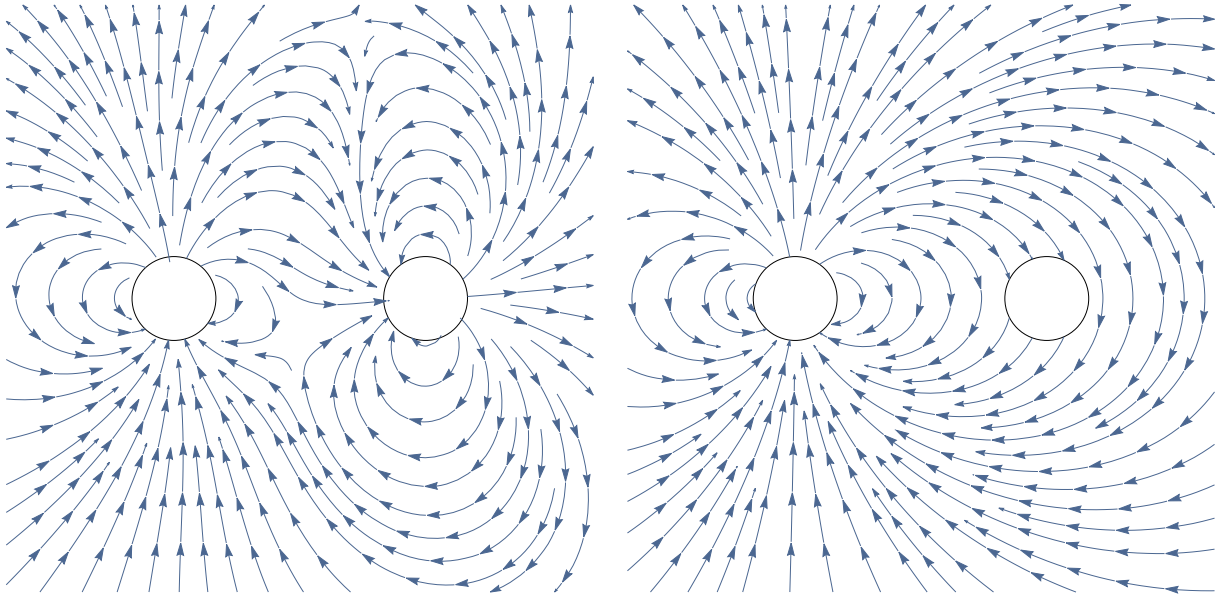


Fig. 8.— Structure of co-rotating reconnected magnetospheres for two orthogonal cases in the $x-z$ plane.

orbital motion in the magnetic field. After a critical value of magnetic bending, instabilities will disrupt the magnetic bridge between. In the process part of the magnetic energy of the flux tube will be dissipated.

The total magnetic energy of a flux tube connecting two stars can be estimated as

$$E_c \approx \frac{B_{NS}^2 R_{NS}^4}{8r_c} = \frac{cI_{NS}^{1/3} B_{NS}^{4/3} R_{NS}^2}{8(GM_{NS})^{1/3} t_{NS}^{1/3}} = 3 \times 10^{38} t_{NS,9}^{-1/3} \text{ erg} \quad (30)$$

This is a fairly small amount of energy, unlikely to be detectable (unless a large fraction is put into radio).

4.7. A step towards a plasma model of interacting magnetospheres

The above considerations were based on the vacuum assumption. Appearance of parallel electric fields, as well as regions with $E > B$, will lead to pair production. As a result the global plasma dynamics will be (could be) described by a plasma (MHD or relativistic force-free) approximation. As a step towards plasma models let us estimate typical current densities and the corresponding charge density.

Two lines of reasoning give the bracketing estimates of the plasma density in the 2M-DNS model. First, the typical current and charge density in the magnetosphere can be estimated as

$$\begin{aligned} I &\sim c\beta B_{or} x_0 \\ j &\sim \frac{I}{\pi x_0^2} \sim B_{or} \Omega / \pi \\ n_{GJ} &\sim \frac{j}{ec} = \frac{B_{or} \Omega}{\pi ec} \end{aligned} \quad (31)$$

which has a clear relation to the Goldreich-Julian density. Density n_{GJ} , Eq. (31), is the charge density we expect in the magnetospheres of interacting neutron stars.

Second, in the time-dependent configuration 2M-DNS, equating typical $\partial_t \mathbf{E}$ to the electric current j (in proper units), we find

$$\begin{aligned} j &\propto B_{NS} \frac{cR_{NS}}{\pi x_0^2} \left(\frac{R_{NS} \Omega}{c} \right)^2 = \frac{B_{or}}{\pi} \frac{GM}{cx_0^2} \\ n_{EM} &= \frac{j}{ec} = \frac{B_{NS}}{\pi ec} \frac{cR_{NS}}{x_0^2} \left(\frac{R_{NS} \Omega}{c} \right)^2 = \frac{B_{or} \Omega}{\pi ec} \sqrt{\frac{r_G}{x_0}} = \beta n_{GJ} \end{aligned} \quad (32)$$

where $r_G = GM/c^2$, $\beta = \sqrt{GM/(c^2 x_0)} = \sqrt{r_G/x_0}$, $B_{or} \sim B_{NS} (R_{NS}/x_0)^{-3}$ is the average magnetic field in the immediate surrounding of the neutron stars, and we used $\Omega \approx \sqrt{GM/x_0^3}$ (recall that x_0 is the (semi)-separation between the stars). Thus, time-dependence induces a weaker requirement on the charge density, similar to the pulsar magnetosphere case.

By the nature of our vacuum approximation, the expected plasma current is fairly distributed. After the plasma is produced, narrow current sheets may/will be formed, leading to intermittent, and possibly explosive relativistic reconnection (Lyutikov & Uzdensky 2003; Lyutikov et al.

2017a,b), particle acceleration, and production of the non-thermal radiation. Thus, we expect that magnetospheric interaction produces flares.

4.8. The last few minutes: possible compactness shroud

As the neutron stars spiral in, the potential and the total luminosity increase. As some point before the merger the compactness parameter,

$$l_c = \frac{\sigma_T L_2}{4\pi r^2 m_e c^3} = \frac{2 e^4 G M_{NS} B_{NS}^2 R_{NS}^6}{3 m_e^3 c^8 r^6} = \frac{2}{3} \frac{e^4 B_{NS}^2 R_{NS}^6}{c^{1/2} (G M_{NS})^{7/2} m_e^3 c^8 (-t)^{3/2}} = 3 \times 10^6 (-t)^{-3/2} \quad (33)$$

becomes larger than unity. This occurs at

$$\begin{aligned} r_c &= \frac{e^{2/3} B_{NS}^{1/3} R_{NS} (G M_{NS})^{1/6}}{c^{4/3} m_e^{1/2}} = 5 \times 10^7 \text{ cm} \\ -t_c &= \frac{e^{8/3} B_{NS}^{4/3} R_{NS}^4}{c^{1/3} m_e^2 (G M_{NS})^{7/3}} = 2 \times 10^4 \text{ sec.} \end{aligned} \quad (34)$$

Qualitatively, when the compactness parameter becomes larger than unity a large fraction of energy is converted into pairs that form an optically dense plasma that in turn may shroud the central neutron stars (Metzger & Zivancev 2016).

If the shrouding indeed occurs, this will be a bad news for a possibility to observe the precursors, since (i) the luminosity of the expected GRB-like outflow from the shroud will be small - of the total luminosity (23), which is already small, most energy will be spent on flow acceleration and not on the production of emission (recall the low efficiency problem of early theories of GRB outflows Goodman 1986); (ii) the shroud will redistribute possibly directed emission from gaps/reconnection sites into isotropic fireball, preventing orbital modulation; (iii) shrouding is likely to pollute the gaps and prevent generation of coherent radio emission.

It is far from clear that shrouding would indeed occur since the estimate (33): (i) is based on the total Poynting luminosity, the real electromagnetic luminosity will be smaller, resulting in smaller l_c ; assumes that most of the luminosity initially comes out in pair-producing photons with energy ≥ 1 MeV; assumes that radiation processes are isotropic - anisotropic particle acceleration in the gaps/current sheets will produce anisotropic photon distribution which will reduce pair production efficiency.

5. Discussion

In this paper we argue that an effective “friction” of the of magnetospheres due to the orbital motion can revive pair production and lead to generation of electromagnetic emission. We demonstrate that the interaction of the magnetic fields of the merging neutron stars can create vacuum

gaps, somewhat akin to the outer gaps in pulsar magnetospheres (Cheng et al. 1986; Romani 1996), and reconnection sheets. The total available potentials in merging neutron stars (Eqns. (7)-(23)) are larger than what is needed to produce pairs (sufficiently close to the merger), these parallel electric fields, and regions with $E > B$, will result in pair production, that will screen them, and reduce the problem to the plasma case of $\mathbf{E} \cdot \mathbf{B} \approx 0$. In the process, this will (may) create particle distributions that are unstable to the generation of radio waves.

The problem of pulsar radio emission - generation of radio waves by a relativistic unipolar inductor - is notoriously complicated. It is a general agreement that parallel electric fields are needed. Particles will be accelerated in the gaps, and under certain conditions can generate a dense secondary pair plasma. Plasma instabilities (*e.g.* Melrose 1989; Lyutikov et al. 1999; Melrose 2000) then may lead to the generation of coherent radio emission.

The active stage of the DNS merger, when LIGO gets an appreciable signal, lasts for ~ 100 seconds (Abbott et al. 2017); hence there may be enough time for radio observations, *e.g.* with LOFAR. LOFAR can see the whole sky at a given time, especially with its low frequency antennas (LBAs, 10-90MHz); the high frequency antennas (HBAs, 110-240MHz) can see the ~ 20 degree-wide field. The data rate is huge, so that phase correlations are mostly done in real time; there is a possibility to have data stored using the Transient Buffer Boards, to be linked to transients' notifications. The low frequency radio waves can also be delayed by \sim tens of seconds due to plasma dispersion effects, possibly giving extra time for responses to the notification of a transient.

Acknowledgments

This work had been supported NSF grant AST-1306672, DoE grant DE-SC0016369 and NASA grant 80NSSC17K0757.

ML would like to thank Dimitrios Giannios, Jason Hessels, Stephen Reynolds and Joeri van Leeuwen for discussions, and organizers and participants of the Plasma Physics of Neutron Star Mergers workshop.

REFERENCES

- Abbott, B. P., Abbott, R., Abbott, T. D., Acernese, F., Ackley, K., Adams, C., Adams, T., Addesso, P., Adhikari, R. X., Adya, V. B., & et al. 2017, Physical Review Letters, 119, 161101
- Baiotti, L., & Rezzolla, L. 2017, Reports on Progress in Physics, 80, 096901
- Bildsten, L., & Cutler, C. 1992, ApJ, 400, 175

- Blandford, R. D. 2002, in *Lighthouses of the Universe: The Most Luminous Celestial Objects and Their Use for Cosmology*, ed. M. Gilfanov, R. Sunyaev, & E. Churazov, 381
- Cheng, K. S., Ho, C., & Ruderman, M. 1986, *ApJ*, 300, 500
- de Jager, O. C., Harding, A. K., Michelson, P. F., Nel, H. I., Nolan, P. L., Sreekumar, P., & Thompson, D. J. 1996, *ApJ*, 457, 253
- Fawley, W. M., Arons, J., & Scharlemann, E. T. 1977, *ApJ*, 217, 227
- Gehrels, N. *et al.* . 2004, *ApJ*, 611, 1005
- Goldreich, P., & Julian, W. H. 1969, *ApJ*, 157, 869
- Goodman, J. 1986, *ApJ*, 308, L47
- Hansen, B. M. S., & Lyutikov, M. 2001, *MNRAS*, 322, 695
- Hirschman, J. A., & Arons, J. 2001, *ApJ*, 560, 871
- Lai, D. 2012, *ApJ*, 757, L3
- Levinson, A., Melrose, D., Judge, A., & Luo, Q. 2005, *ApJ*, 631, 456
- Lyutikov, M. 2006, *New Journal of Physics*, 8, 119
- . 2011a, *Phys. Rev. D*, 83, 124035
- . 2011b, *Phys. Rev. D*, 83, 064001
- Lyutikov, M., Komissarov, S., & Sironi, L. 2018, *Journal of Plasma Physics*, 84, 635840201
- Lyutikov, M., Machabeli, G., & Blandford, R. 1999, *ApJ*, 512, 804
- Lyutikov, M., Sironi, L., Komissarov, S. S., & Porth, O. 2017a, *Journal of Plasma Physics*, 83, 635830601
- . 2017b, *Journal of Plasma Physics*, 83, 635830602
- Lyutikov, M., & Uzdensky, D. 2003, *ApJ*, 589, 893
- Melrose, D. B. 1989, *Instabilities in Space and Laboratory Plasmas*, ed. D. B. Melrose
- Melrose, D. B. 2000, in *Astronomical Society of the Pacific Conference Series*, Vol. 202, IAU Colloq. 177: *Pulsar Astronomy - 2000 and Beyond*, ed. M. Kramer, N. Wex, & R. Wielebinski, 721–+
- Metzger, B. D., & Zivancev, C. 2016, *MNRAS*, 461, 4435
- Misner, C. W., Thorne, K. S., & Wheeler, J. A. 1973, *Gravitation* (San Francisco: W.H. Freeman and Co., 1973)

- Palenzuela, C., Lehner, L., & Liebling, S. L. 2010, *Science*, 329, 927
- Palenzuela, C., Lehner, L., Liebling, S. L., Ponce, M., Anderson, M., Neilsen, D., & Motl, P. 2013a, *Phys. Rev. D*, 88, 043011
- Palenzuela, C., Lehner, L., Ponce, M., Liebling, S. L., Anderson, M., Neilsen, D., & Motl, P. 2013b, *Physical Review Letters*, 111, 061105
- Ponce, M., Palenzuela, C., Barausse, E., & Lehner, L. 2015, *Phys. Rev. D*, 91, 084038
- Ponce, M., Palenzuela, C., Lehner, L., & Liebling, S. L. 2014, *Phys. Rev. D*, 90, 044007
- Romani, R. W. 1996, *ApJ*, 470, 469
- Tan, C. M., Bassa, C. G., Cooper, S., Dijkema, T. J., Esposito, P., Hessels, J. W. T., Kondratiev, V. I., Kramer, M., Michilli, D., Sanidas, S., Shimwell, T. W., Stappers, B. W., van Leeuwen, J., Cognard, I., Gri  meier, J.-M., Karastergiou, A., Keane, E. F., Sobey, C., & Weltevrede, P. 2018, *ArXiv e-prints*
- Timokhin, A. N. 2010, *MNRAS*, 408, 2092
- Uchida, Y., & Sakurai, T. 1983, in *Astrophysics and Space Science Library*, Vol. 102, IAU Colloq. 71: Activity in Red-Dwarf Stars, ed. P. B. Byrne & M. Rodono, 629–632